Nonlinear Dyn (2012) 69:1679–1692
DOI 10.1007/s11071-012-0378-2

ORIGINAL PAPER

Parametric resonances in a base-excited double pendulum

J.C. Sartorelli · W. Lacarbonara

Received: 2 June 2011 / Accepted: 18 February 2012 / Published online: 15 March 2012

Abstract Two parametrically-induced phenomena are addressed in the context of a double pendulum subject to a vertical base excitation. First, the parametric resonances that cause the stable downward vertical equilibrium to bifurcate into large-amplitude periodic solutions are investigated extensively. Then the stabilization of the unstable upward equilibrium states through the parametric action of the high-frequency base motion is documented in the experiments and in the simulations. It is shown that there is a region in the plane of the excitation frequency and amplitude where all four unstable equilibrium states can be stabilized simultaneously in the double pendulum.

The parametric resonances of the two modes of the base-excited double pendulum are studied both theoretically and experimentally. The transition curves (i.e., boundaries of the dynamic instability regions) are constructed asymptotically via the method of multiple scales including higher-order effects. The bifurcations characterizing the transitions from the trivial equilibrium to the periodic solutions are computed by either continuation methods and or by time integration and compared with the theoretical and experimental results.

Keywords Double pendulum · Parametric resonance · Transition curves · Method of multiple scales · High-frequency excitation

J.C. Sartorelli (✉)
Universidade de São Paulo, Instituto de Física, Caixa Postal 66318, 05314-970 São Paulo, Brazil
e-mail: sartorelli@if.usp.br

W. Lacarbonara
Dipartimento di Ingegneria Strutturalem, Universitá Degli Studi di Roma La Sapienza, Via Eudossiana 18, 00184 Roma, Italy
e-mail: walter.lacarbonara@uniroma1.it

1 Introduction

Parametric resonances are often encountered in mechanics (e.g., dynamic buckling of columns, plates and shells, water waves in vertically forced containers, stability of general motions) and in various areas of physics. Faraday [1] was the first to observe the phenomenon of parametric resonance in surface waves of a fluid-filled cylinder under vertical excitation which exhibited twice the period of the excitation. Lord Rayleigh [2] provided a theoretical foundation for interpreting the parametric resonance of strings.

Various works have dealt with the parametric resonance of the simple pendulum due to its paradigmatic nature and simplicity for experimental studies. For small-amplitude oscillations, the equation of motion reduces to Hill's equation, $\ddot{\theta} + [\omega^2 + \ddot{y}/l]\theta = 0$, where $\ddot{y}$ is the prescribed vertical acceleration of the pivot, θ is the angle measured from a fixed vertical line, and ω is the natural frequency of the pendulum. If the base excitation is harmonic, $y = Y \cos \Omega t$, this equation is referred to as Mathieu's equation [3, 4].

The associated instability regions emanate from the critical frequencies $\Omega = \frac{2}{m}\omega$, $m = 1, 2, \ldots$, on the Ω-axis in the (Ω, Y)-plane. The first instability region for $m = 1$, which emanates from $\Omega = 2\omega$, is the *principal parametric resonance*. The second instability region, for $m = 2$, corresponds to $\Omega = \omega$, and is referred to as *parametric resonance*. The other regions correspond to higher-order resonances, such as $\Omega = \frac{2}{3}\omega$, $\frac{1}{2}\omega$, $\frac{2}{5}\omega$, etc., and thus accumulate on the origin of the frequency axis at $\Omega = 0$ as m goes to ∞.

Some features of the chaotic dynamics of the single pendulum were discussed in [5, 6], while [7] and [8] addressed the forced double pendulum and the triple pendulum, respectively. For small forcing amplitudes, there are many theoretical studies dealing with parametric resonances in the planar double pendulum [9–13]. In particular, El-Bassiouny [12] employed the method of multiple scales to study the principal parametric resonance of both in-phase and out-of-phase modes of a double pendulum. He found that each mode has a single-valued curve and there exist multi-valued zones upon varying some parameters. Both modes can lose their stability.

Experimental studies about double pendulums have considered several different geometric configurations as well as forcing conditions. An orthogonal pendulum whose lower arm oscillates in a plane orthogonal to that of the upper arm was considered in [14], while [15] addressed the transition from planar to orthogonal configurations. Studies of the motions of a double pendulum, excited by the rotation of the lower arm attached through a dc motor to the end of the upper arm, were presented in [16]. Liang and Feeny [17] investigated the parametric identification of a chaotic system represented by a double pendulum. They extracted the unstable periodic orbits from recorded experimental data which were then used within an identification process based on the harmonic balance method.

The effects of follower forces in inverted double pendulums (with rotational springs and dashpots between the arms), subject to base excitations, have been studied in depth. Jensen [18] investigated the effects of small-amplitude resonant high-frequency excitation on the linear stability and nonlinear behavior of the pendulum by using the method of direct partition of motion due to Blekhman [19]. He showed that the support excitation has a stabilizing effect for most system parameters but can also destabilize the upright pendulum position, supercritical bifurcations may turn into subcritical bifurcations and chaotic behaviors of the pendulum exist for a wide range of system parameters and initial conditions. In a similar system, Yu and Bi [20] used normal form and bifurcation theory to find closed-form solutions for equilibria, periodic and quasi-periodic motions.

Existence, bifurcations, and stability of high-frequency periodic motions of a double pendulum were studied in [21]. The linear stability analysis of the four equilibria was carried out for generic geometries, although when the two arms are identical the stability problem could be studied in the full nonlinear setting. A rigorous nonlinear analysis of the existence and stability of periodic motions of the mathematical pendulum—under various horizontal and oblique motions of the suspension point—can be found in [22]. For the case of vertical base excitations at an arbitrary frequency and amplitude, a stability analysis of the equilibria of the double pendulum was carried out in [23]. Along the same lines, a large body of works has addressed high-frequency parametric excitations [3, 19].

In the present work, we first aim to study the parametric instability regions via the method of multiple scales—previously employed in the context of various parametric resonances of two-degree-of-freedom systems and cantilever beams [24, 25]. This effort follows along the lines of recent investigations [26]. Secondly, we aim to study numerically and experimentally (i) the onset of the parametric instability for both modes, (ii) the post-critical motions and the underlying bifurcations, and (iii) the possibility of stabilization of all unstable equilibria via the high-frequency parametric excitation phenomenon.

The investigated parametrically excited double pendulum has two arms of about the same length, although arm 1 is heavier than arm 2 ($m_1 \sim 3.5 m_2$). The frequencies of the two modes are $f_1 = 1.44$ Hz (in-phase mode) and $f_2 = 2.42$ Hz (out-of-phase mode). The equilibrium solutions are given by $\theta_i^{\mathrm{o}} = k_i \pi$, where $k_i = 0, 1, 2, \ldots$. For conciseness, they will be referred to as the four fixed points $(\theta_1^{\mathrm{o}}, \theta_2^{\mathrm{o}}) = (0, 0)$, $(0, \pi)$, $(\pi, 0)$, and (π, π).

When the suspension point is forced periodically in the vertical direction by the prescribed motion $y(t) = Y \cos \Omega t$, the double pendulum dynamics exhibit interesting phenomena such as the parametric resonances of the two modes which give rise to large-amplitude pendulations or the stabilization of all un-

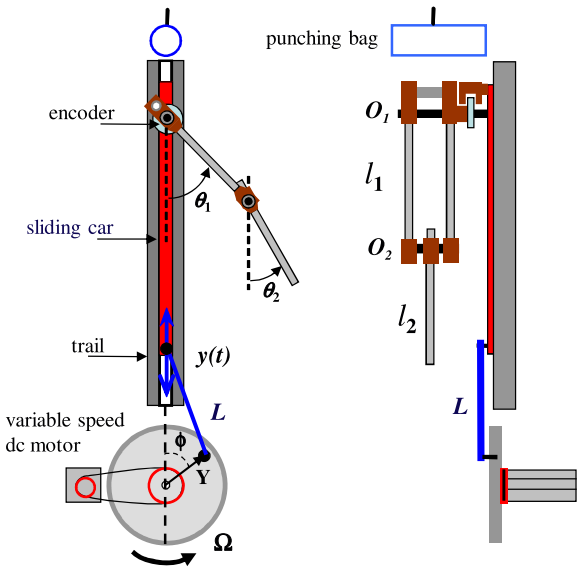

Fig. 1 Front view of the double pendulum (*left*) and lateral view (*right*). Parameter values: $l_1 = 10.86$ cm, $m_1 = 18.45$ g, $J_1^{\mathrm{o}} = 0.7149\,\mathrm{g\,cm^2}$, center of mass $l_1^{\mathrm{c}} = 4.20$ cm, $l_2 = 9.50$ cm, $m_2 = 5.32$ g, $J_2^{\mathrm{o}} = 79.4\,\mathrm{g\,cm^2}$, $l_2^{\mathrm{c}} = 2.41$ cm, handle length $L = 22.5$ cm, $Y^{\max} = 4$ cm

stable fixed points depending on the excitation frequency $f = \Omega/(2\pi)$ and amplitude Y. The stabilization of the upright (unstable) positions (e.g., via feedback control laws [27]) or the cancellation of the parametric resonances (e.g., via open-loop laws [28]) have been widely investigated in the literature.

2 Theoretical analysis

The equations of motion of a double pendulum subject to a vertical base motion $y(t)$ (see Fig. 1) are described by the following two ordinary differential equations with time-varying coefficients:

$$J_1\ddot{\theta}_1 + I_1(g+\ddot{y})\sin\theta_1 + c_1\dot{\theta}_1 + I_2^{\mathrm{o}} l_1 \ddot{\theta}_2 \cos(\theta_1-\theta_2) + I_2^{\mathrm{o}} l_1 \sin(\theta_1-\theta_2)\dot{\theta}_2^2 = 0, \tag{1}$$

$$J_2^{\mathrm{o}}\ddot{\theta}_2 + I_2^{\mathrm{o}}(g+\ddot{y})\sin\theta_2 + c_2\dot{\theta}_2 + I_2^{\mathrm{o}} l_1 \ddot{\theta}_1 \cos(\theta_1-\theta_2) - I_2^{\mathrm{o}} l_1 \sin(\theta_1-\theta_2)\dot{\theta}_1^2 = 0 \tag{2}$$

where θ_1 and θ_2 are the angles of the upper and lower arms, respectively, measured from a fixed vertical line (taken positive when they are counterclockwise); the overdot indicates differentiation with respect to time. The system parameters are expressed as: $J_1 := J_1^{\mathrm{o}} + m_2 l_1^2$, $I_k^{\mathrm{o}} := m_k l_k^{\mathrm{c}}$, $I_1 := I_1^{\mathrm{o}} + l_1 m_2$, where m_k, l_k, l_k^{c}, J_k^{o} $(i = 1, 2)$ denote the masses, the arm lengths, the distances of the center of mass of the kth arm from O_k, and the moments of inertia about O_k (see Fig. 1 for the parameter values of the experimental setup). (I_k, J_k) represent first- and second-order mass moments of inertia of the kth arm. Equations of motion (1) and (2) describe a double pendulum with generic nonuniform mass properties of the arms as in many practical applications. Equations of motion (1) and (2) were obtained by applying Euler–Lagrange's equations to the system Lagrangian and employing the Rayleigh dissipation function to incorporate the nonconservative linear damping forces. The equations of motion exhibit inertia nonlinearities together with the base-excitation-related multiplicative terms featuring nonlinear coupling of the base motion with the motion of the pendulum arms.

We nondimensionalize time as $t^* = \omega_c t$, with $\omega_c^2 := g/l$ and $l := l_1 + l_2$, where the superscript star indicates nondimensional variables, g is the gravity acceleration. Thus ω_c has the meaning of circular frequency of a simple pendulum with length equal to the sum of the lengths of the two arms. The following nondimensional parameters are accordingly defined: $\alpha := I_1 l/J_1$, $\beta := I_2^{\mathrm{o}} l/J_1$, $\rho := J_2^{\mathrm{o}}/J_1$, $\delta := l_1/l$. The nondimensional amplitude and frequency of the prescribed periodic base motion, $y(t) = Y\cos\Omega t$, are $Y^* := Y/l$ and $\Omega^* := \Omega/\omega_c$, respectively. The equations of motion in nondimensional form thus become

$$\ddot{\theta}_1 + \alpha\big[1+\ddot{y}(t)\big]\sin\theta_1 + \xi_1\dot{\theta}_1 + \beta\delta\ddot{\theta}_2\cos(\theta_1-\theta_2) + \beta\delta\sin(\theta_1-\theta_2)\dot{\theta}_2^2 = 0, \tag{3}$$

$$\rho\ddot{\theta}_2 + \beta\big[1+\ddot{y}(t)\big]\sin\theta_2 + \xi_2\dot{\theta}_2 + \beta\delta\ddot{\theta}_1\cos(\theta_1-\theta_2) - \beta\delta\sin(\theta_1-\theta_2)\dot{\theta}_1^2 = 0, \tag{4}$$

where $\xi_k := (c_k/J_1)\sqrt{l/g}$ are nondimensional damping coefficients and the stars were dropped for the sake of notational simplicity. Thus the double pendulum, without damping, is governed by the following four independent parameters: $(\alpha, \beta, \delta, \rho)$.

Without the forcing term, under the mere action of gravity, the double pendulum exhibits four equilibria (fixed points), namely $(\theta_1^{\mathrm{o}}, \theta_2^{\mathrm{o}}) = (0,0), (0,\pi), (\pi,0), (\pi,\pi)$, of which only $(0,0)$ is stable (marginally or

asymptotically depending on the absence or presence of damping). The double pendulum possesses two vibration modes about the stable equilibrium $(0,0)$ of which the lowest represents the in-phase mode while the second is the out-of-phase mode. The frequencies and eigenvectors associated with these modes are given by

$$\omega_{1,2} = \sqrt{-\frac{\alpha\rho + \beta \mp \sqrt{\alpha^2\rho^2 + 4\alpha\beta^3\delta^2 - 2\alpha\beta\rho + \beta^2}}{2\beta^2\delta^2 - 2\rho}}, \tag{5}$$

$$\mathbf{u}_{1,2} = \left[\pm\frac{\sqrt{\alpha^2\rho^2 + 4\alpha\beta^3\delta^2 - 2\alpha\beta\rho + \beta^2} \mp \alpha\rho \pm \beta}{2\alpha\beta\delta}, 1\right]^\top, \tag{6}$$

where $\top$ indicates the transpose. The eigenvectors $\mathbf{u}_k = [\theta_1, \theta_2]^\top$ are then normalized according to $\mathbf{u}_k^\top \mathbf{M}\mathbf{u}_k = 1$ and the normalized components are denoted by u_{k1} and u_{k2}, respectively.

The physical parameters of the double pendulum used for the experiments are: $l_1 = 10.865$ cm, $l_2 = 9.5$ cm, $m_1 = 18.45 \times 10^{-3}$ kg, $m_2 = 5.32 \times 10^{-3}$ kg, $l_1^c = 4.20$ cm, $l_2^c = 2.41$ cm, $J_1^o = 0.71431$ kg cm^2, $J_2^o = 0.07940$ kg cm^2. The gravity acceleration (measured in São Paulo) is $g = 9.78$ m/s^2. The corresponding nondimensional parameters are given by $\rho = 0.0592$, $\alpha = 2.053$, $\beta = 0.1945$, and $\delta = 0.5335$. Due to the uncertainty inherent in the level of dissipation (due to dry friction in the hinges of the pivot points and air drag), three values of the damping coefficients are considered: $c_1 = c_2 = (0.015, 0.15, 0.5)$ kg cm^2/s. The corresponding nondimensional damping coefficients are $\xi_1 = \xi_2 = (0.161, 1.61, 5.37) \times 10^{-2}$ while the associated modal damping factors are $\zeta_k := \xi_k/(2\omega_k) = (0.06, 0.62, 2.05)$ % for mode 1 and $(0.037, 0.37, 1.22)$ % for mode 2, respectively.

The frequencies of the two modes calculated according to (5) are 1.44 Hz and 2.42 Hz, respectively. Due to the fact that the arms are not uniform, the moments of inertia are determined using a linear system identification technique. To this end, let us consider the equation of a single pendulum given by

$$J_k\ddot{\theta}_k + m_k l_k^c g \sin\theta_k = 0 \tag{7}$$

whose period of small oscillations is given by

$$T_k = 2\pi\sqrt{J_k/\left(m_k l_k^c g\right)}. \tag{8}$$

By measuring the position of the center of mass (l_k^c) and the oscillation period (T_k), the moment of inertia J_k can be determined solving (8).

When the frequency of the base excitation Ω is close to twice the natural frequency of one of the two pendulum modes, the pendulum can undergo a principal parametric instability. An asymptotic treatment by the method of multiple scales is presented next. Closed-form expressions of the transition curves in the parameter plane (f, Y) are obtained for different levels of damping.

2.1 Perturbation analysis

Uniform asymptotic expansions of the resonant periodic motions by the method of multiple scales [29] are sought when $\Omega \simeq 2\omega_k$, $k = 1, 2$. To this end, we introduce a small nondimensional bookkeeping parameter ε and rescale the nondimensional damping coefficient and the base excitation amplitude as $\epsilon^2\xi_k$ and $\epsilon^2 Y$. The equations of motion are then expanded in Taylor series about $(\theta_1, \dot{\theta}_1, \theta_2, \dot{\theta}_2) = (0, 0, 0, 0)$ up to fifth polynomial degree thus obtaining

$$\begin{aligned}
&\ddot{\theta}_1 + \beta\delta\ddot{\theta}_2 + \alpha\theta_1 + \epsilon^2\xi_1\dot{\theta}_1 + \epsilon^2\alpha y(t)\theta_1 \\
&\quad - \frac{1}{6}\alpha\left[1 + \epsilon^2 q(t)\right]\theta_1^3 + \beta\delta(\theta_1 - \theta_2)\dot{\theta}_2^2 \\
&\quad - \frac{1}{2}\beta\delta\left(\theta_1^2 + \theta_2^2\right)\ddot{\theta}_2 + \beta\delta\theta_1\theta_2\ddot{\theta}_2 \\
&\quad + \frac{1}{24}\beta\delta\left(\theta_1^4 + \theta_2^4\right)\ddot{\theta}_2 + \frac{1}{4}\beta\delta\theta_1^2\theta_2^2\ddot{\theta}_2 \\
&\quad - \frac{1}{6}\beta\delta\left(\theta_1\theta_2^3 + \theta_1^3\theta_2\right)\ddot{\theta}_2 + \frac{1}{2}\beta\delta\left(\theta_1^2\theta_2 - \theta_1\theta_2^2\right)\dot{\theta}_2^2 \\
&\quad + \frac{1}{6}\beta\delta\left(\theta_2^3 - \theta_1^3\right)\dot{\theta}_2^2 + \frac{1}{120}\alpha\theta_1^5 = 0,
\end{aligned} \tag{9}$$

$$\begin{aligned}
&\rho\ddot{\theta}_2 + \beta\delta\ddot{\theta}_1 + \beta\theta_2 + \epsilon^2\xi_2\dot{\theta}_2 + \epsilon^2\beta y(t)\theta_2 \\
&\quad - \frac{1}{2}\beta\delta\theta_2^2\ddot{\theta}_1 + \beta\delta\theta_1\theta_2\ddot{\theta}_1 + \beta\delta(\theta_2 - \theta_1)\dot{\theta}_1^2 \\
&\quad - \frac{1}{6}\beta\left[1 + \epsilon^2 q(t)\right]\theta_2^3 + \frac{1}{24}\beta\delta\left(\theta_1^4 + \theta_2^4\right)\ddot{\theta}_1 \\
&\quad - \frac{1}{6}\beta\delta\theta_1\theta_2^3\ddot{\theta}_1 + \frac{1}{4}\beta\delta\theta_1^2\theta_2^2\ddot{\theta}_1 - \frac{1}{6}\beta\delta\theta_1^3\theta_2\ddot{\theta}_1 \\
&\quad - \frac{1}{6}\beta\delta\left(\theta_2^3 + \theta_1^3\right)\dot{\theta}_1^2 + \frac{1}{2}\beta\delta\left(\theta_1\theta_2^2 - \theta_1^2\theta_2\right)\dot{\theta}_1^2 \\
&\quad + \frac{1}{120}\beta\theta_2^5 = 0.
\end{aligned} \tag{10}$$

To treat (9) and (10) by the method of multiple scales [29], we introduce the time scales $t_0 := t,\ t_2 := \varepsilon^2 t,\ t_4 := \varepsilon^4 t$. The time scale t_0 accounts for the rapidly varying part of the motion (occurring at the natural frequencies) and the stretched time scales t_2 and t_4 account for the slowly-varying part of the motion. We introduce only three time scales because we terminate the perturbation procedure at fifth order. A one-term expansion is obtained by carrying out the analysis up to the cubic order where the solvability condition gives the modulation equations. A two-term expansion is obtained by carrying out the analysis up to the quintic order.

Provided that the data are sufficiently smooth, we seek asymptotic expansions of the solutions in the form

$$\theta_k(t,\varepsilon) \sim \sum_{j=1}^{5} \theta_{k,j}(t,t_2,t_4)\varepsilon^j \tag{11}$$

where the functions $\theta_{k,j}(t_0,t_2,t_4)$ are to be determined. Thus

$$\begin{aligned} \frac{d}{dt} &\sim \left[D_0 + \varepsilon^2 D_2 + \varepsilon^4 D_4\right], \\ \frac{d^2}{dt^2} &\sim \left[D_0^2 + 2\varepsilon^2 D_0 D_2 + \varepsilon^4\left(2D_0 D_4 + D_2^2\right)\right] \end{aligned} \tag{12}$$

where $D_n(\cdot) := \partial(\cdot)/\partial t_n$. To express the closeness of the resonance condition, we let $\Omega = 2\omega_k + \varepsilon^2\lambda$ and account for the fact that, to within second order, the base acceleration is expressed as

$$\begin{aligned} \ddot{y} &= \left[D_0^2 + 2\varepsilon^2 D_0 D_2\right]\frac{1}{2} Y\left[e^{i(2\omega_k t_0 + \lambda t_2)} + cc\right] \\ &= -4\omega_k Y\left(\omega_k + \varepsilon^2\lambda\right)\frac{1}{2}\left(e^{i\Omega t_0} + cc\right). \end{aligned} \tag{13}$$

The perturbation at the nth order (with n odd and such that $n \le 5$) is obtained substituting (11) and (12) into the equations of motion (9) and (10) and collecting terms of like powers of ε^n. The problem at $\mathrm{O}(\varepsilon)$ is the linearized eigenvalue problem. Since we seek the expansion of the principal parametric resonance of the kth mode, the generating solution is taken in the form

$$[\theta_{1,1}, \theta_{1,2}]^\top = \mathbf{u}_k\left(A_k e^{i\omega_k t_0} + cc\right) \tag{14}$$

where $A_k(t_2,t_4)$ is the complex-valued amplitude of the motion and cc indicates the complex conjugate of the preceding term. We then substitute (14) into the problem at third order whose solvability, by the Fredholm Alternative Theorem, yields the complex-valued modulation equation

$$D_2 A_k = -\frac{1}{2}\mu_k A_k + i\Gamma_k A_k^2 \bar{A}_k + iY\Lambda_k \bar{A}_k e^{i\lambda t_2} \tag{15}$$

where $(\mu_k, \Gamma_k, \Lambda_k)$ are given by

$$\begin{aligned} \mu_k &= \xi_1 u_{k1}^2 + \xi_2 u_{k2}^2, \\ \Lambda_k &= -\omega_k\left(\alpha u_{k1}^2 + \beta u_{k2}^2\right), \end{aligned} \tag{16}$$

$$\begin{aligned} \Gamma_k = &-\left(\alpha u_{k1}^4 + \beta u_{k2}^4\right)/(4\omega_k) \\ &+ \beta\delta\omega_k\left[u_{k2}u_{k1}^3 - 2u_{k2}^2 u_{k1}^2 + u_{k2}^3 u_{k1}\right]. \end{aligned} \tag{17}$$

The coefficients $(\Gamma_k,\ \Lambda_k)$ are known as the effective nonlinearity coefficient (i.e., it regulates the bending of the backbone of the pendulum mode [29]) and effective parametric resonance coefficient, respectively.

If the perturbation is arrested at this order, by considering $\dot{A} = \varepsilon^2 D_2 A$ and introducing the polar form for the complex-valued amplitude A as $A = \frac{1}{2}a\exp(i\phi/2)\exp(i\lambda t_2)$ into the solvability condition (15), we obtain the coupled ordinary-differential equations that govern the slow time-evolution of the amplitude and phase as

$$\dot{a} = -\frac{1}{2}\mu_k a + \Lambda_k a \sin\phi, \tag{18}$$

$$\dot{\phi} = -\lambda + \frac{1}{2}\Gamma_k a^2 + 2Y\Lambda_k \cos\phi. \tag{19}$$

The amplitude and phase of the 2-periodic solutions emanating from the parametric instability are solutions of $\dot{a} = 0$ and $\dot{\phi} = 0$. The equation relating the amplitude of the motion a, the base excitation Y, and the bifurcation parameter λ is obtained in the form:

$$\lambda = \frac{1}{2}\Gamma_k a^2 \pm \sqrt{4Y^2\Lambda_k^2 - \mu_k^2}. \tag{20}$$

Equation (20) can be expressed in terms of the frequency as

$$\Omega(\varepsilon) = 2\omega_k + \varepsilon^2\left[\frac{1}{2}\Gamma_k a^2 \pm \sqrt{4Y^2\Lambda_k{}^2 - \mu_k{}^2}\right]. \tag{21}$$

The bifurcation equation (20) implies that the parametric instability is initiated only if the base excitation amplitude Y is such that the argument of the square root is positive, that is, $Y \ge Y_k^{\mathrm{c}}$ where Y_k^{c} is the critical amplitude for the onset of the instability in the kth

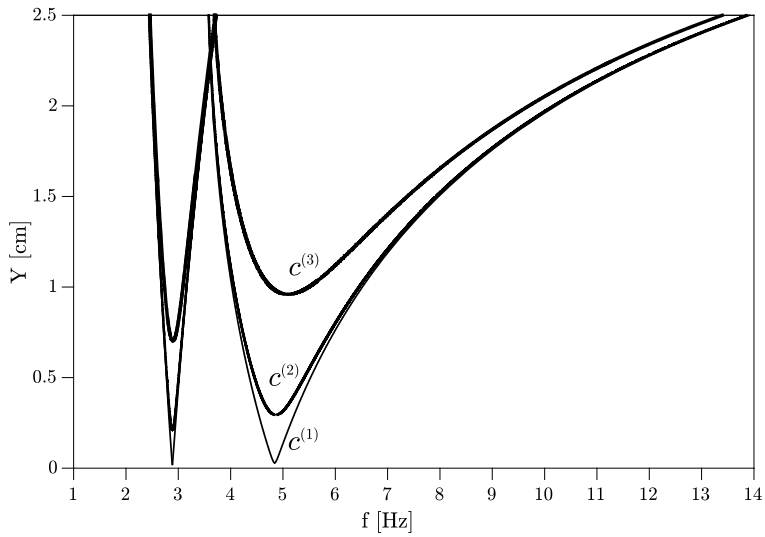

Fig. 2 Principal parametric instability regions of the double pendulum with $l_1 = 10.865$ cm, $l_2 = 9.5$ cm, $m_1 = 18.45$ g, $m_2 = 5.32$ g, $l_1^{\mathrm{c}} = 4.20$ cm, $l_2^{\mathrm{c}} = 2.41$ cm, $J_1^{\mathrm{o}} = 714.31$ g cm^2, $J_2^{\mathrm{o}} = 79.405$ g cm^2, $c_1 = c_2 = c^{(\mathrm{n})}$, with $c^{(1)} = 15$ g cm^2/s, $c^{(2)} = 150$ g cm^2/s, $c^{(3)} = 500$ g cm^2/s

mode:

$$Y_{\mathrm{k}}^{\mathrm{c}} = \frac{\mu_k}{2|\Lambda_k|} = \frac{\xi_1 u_{k1}^2 + \xi_2 u_{k2}^2}{2\omega_k(\alpha u_{k1}^2 + \beta u_{k2}^2)}. \tag{22}$$

An explicit expression for the local approximation of the transition curves around the tip can be obtained from (20) by putting $a = 0$, solving for Y, and expanding the resulting formula about $\lambda = 0$. When the pendulum is fully undamped (i.e., $\mu_k = 0$), the transition curves are obtained from (20) in the form $\Omega = 2\omega_k \pm 2\varepsilon^2 Y \Lambda_k$. Consequently, the transition curve emanates directly from the Ω-axis at $\Omega = 2\omega_k$.

We further carry out the perturbation analysis to the fifth order so as to extend the range of validity of the formulas for the transition curves to higher excitations away from the exact resonance frequency tuning condition, $\Omega = 2\omega_k$. To this end, after enforcing the solvability of the third-order problem, the particular solution at third order is found and substituted into the fifth-order problem. The solvability condition at fifth order, yielding $D_4 A$, is combined with the condition at third order to obtain the time rate of change of A according to the method of reconstitution by which $\dot{A} = \varepsilon^2 D_2 A + \varepsilon^4 D_4 A$. The complex-valued equation is then transformed in real form in terms of the amplitude a and phase ϕ, and the fixed points of $\dot{a} = 0$ and $\dot{\phi} = 0$ are thus determined. The conducted analysis yields a truly two-term expansion of the pendulum resonant motion featuring linear and cubic nonlinear terms.

Figure 2 shows the theoretically obtained transition curves for three values of the damping coefficients. As expected, the threshold amplitudes of the excitation for the onset of the instabilities increase with the damping coefficients. Secondly, the instability region of the out-of-phase mode is significantly wider than that of the in-phase mode; its widening is such that these regions intersect at frequencies slightly higher than twice the natural frequency of the in-phase mode. Figure 3 shows the comparison between the transition curve obtained via the perturbation approach with that obtained by the Matlab-based numerical continuation package COCO [30]. In spite of the relatively high damping, the agreement is good.

3 Experimental and numerical investigations

The double pendulum employed in the experiments and the associated physical parameter values are portrayed in Fig. 1. Arm 1 consists of two aluminum tubes of diameter $d = 3$ mm attached to phenolic resin blocks. Each phenolic block houses a bearing of 8 mm/4 mm external/internal diameter forming the pivot joints at O_1 and O_2. Transversal aluminum elements connect the two tubes in arm 1. Arm 2 is a single aluminum tube attached to a single phenolic block that houses two bearings with external and internal diameters equal to 6 and 3 mm, respectively.

Pivot O_1 is attached to a cart sliding in a trail whose periodic motion is given by a crankshaft wheel. First,

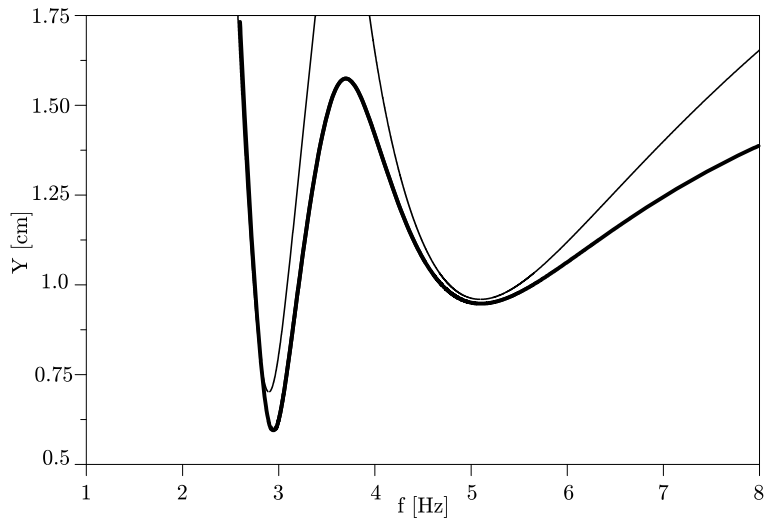

Fig. 3 Principal parametric instability regions of the double pendulum when $c_1 = c_2 = c^{(3)}$: comparison between the perturbation results (*thin line*) and the numerical continuation results (*thick line*)

the excitation amplitude is fixed to its selected value, subsequently measurements are taken so as to change the dc motor speed through digital inputs from the data acquisition system. If Y denotes the radius of the crankshaft wheel, the position of the pivot point of the pendulum is given by

$$y(t) = L\big[1 - \sqrt{1 - (Y/L)^2 \sin^2\phi(t)}\big] + Y\big[1 - \cos\phi(t)\big]. \tag{23}$$

Differentiating it twice with respect to time, setting $\Omega = \dot{\phi}$, and letting $Y/L \ll 1$ yields the acceleration in the form

$$\ddot{y}(t) \sim Y\Omega^2 \cos\Omega t. \tag{24}$$

The range of excitation amplitude Y and frequency $f = \Omega/(2\pi)$ are restricted to [0, 4] cm and to [0, 17] Hz, respectively.

We measured the average of the absolute value of the angular velocity $\omega_1 = \dot{\theta}_1$ of arm 1 detecting the instants of induced pulses through a transmissive optical encoder using an ADC counter at 100 ksamples/s. The angular resolution is $2\pi/2500 \sim 2.5 \times 10^{-3}$ rad, so $|\omega_1| = (2\pi/2500)/\Delta t$, where Δt is the time interval between two successive pulses. The data were recorded after waiting a minimum time of 10 s subsequent to a forcing frequency change (i.e., increment or decrement depending on the sweeping direction).

In Fig. 4 we show the experimental results for the transition curves of the in-phase and out-of-phase modes. The curves were obtained by a forward sweep of the forcing frequency (triangles) followed by a backward sweep (upside down triangles). The loss of stability is encountered at the threshold amplitude $Y_{\min} \sim 0.7$ cm.

The transition curves were also obtained employing the Floquet theory [31] by assuming $\theta_k(t)$ in the form $\theta_k = e^{\lambda t}\cos(\Omega/2\, t + \phi_k)$, where λ is the Floquet exponent, Ω is the (circular) frequency of the base motion, and ϕ_k is the relative phase between the response and the excitation. Moreover, to explore other global phenomena such as the parametrically-driven stabilization of the unstable upward equilibria, a full numerical approach was employed resorting to a direct integration of the equations of motion over a sufficiently large time span taken equal to 2000 s. The time integration was carried out using the variable-step Dormand–Prince algorithm with initial conditions $(\theta_1(0), \theta_2(0)) = (\theta_1^{\mathrm{o}} + \epsilon, \theta_2^{\mathrm{o}} + \epsilon)$ and $(\omega_1(0), \omega_2(0)) = (0, 0)$ (ϵ is a small perturbation of the equilibrium state) and the observed decay of $\theta_1(t)$ and $\theta_2(t)$. To this end, we divided the parameter plane, $f \in [0, 17]$ Hz and $Y \in [0, 4]$ cm, in a lattice of $n_f \times n_Y$ points suitable to capture local variations of the transition curves.

In particular, in Fig. 4(a) the solid black line is the transition curve without damping. Below the solid black line, the equilibrium $(0, 0)$ is stable; above it, the fully developed parametric resonance can lead to periodic solutions or other attractors. In the same figure, the transition curves obtained by the Floquet theory are portrayed as a sequence of gray dots and a

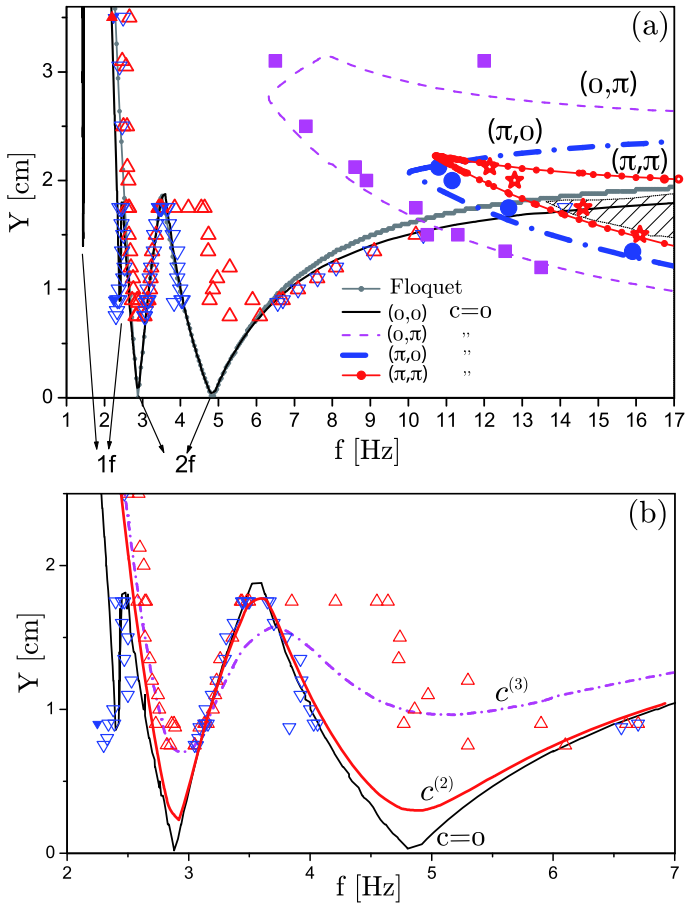

Fig. 4 Transition curves in the (Y, f)-plane for the in-phase and out-of-phase modes. *Regular triangles* (*upside down triangles*) denote forward (*backward*) frequency sweeps. In part (**a**), *squares*, *circles* and *five-point stars* indicate the borders of the fixed points $(0, \pi)$, $(\pi, 0)$, and (π, π), respectively. The simulated curve is numerically obtained without damping (*black line*) as well as through the Floquet theory for the principal parametric resonance (*dashed gray line*). In part (**b**), a zoomed-in view at various damping levels: $c = 0$ (*black line*); $c^{(2)} = 150$ g cm^2/s, (*gray line*), $c^{(3)} = 500$ g cm^2/s (*dashed–dotted line*)

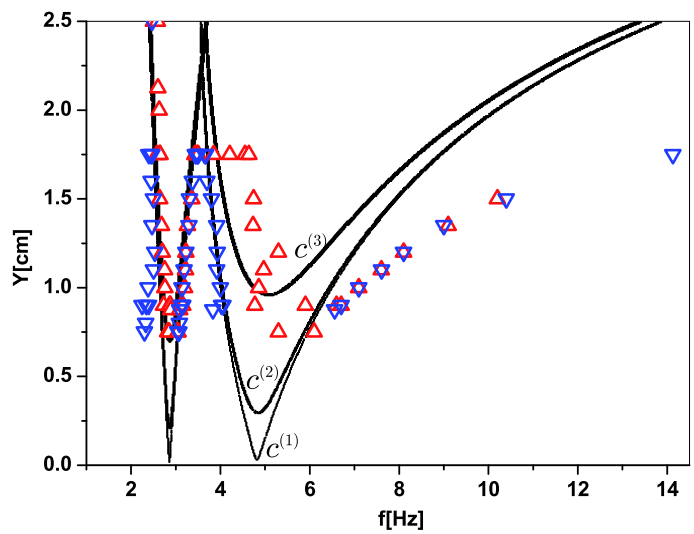

Fig. 5 Comparison between the transition curves obtained theoretically (*solid lines*) for three damping values and those experimentally measured (*triangles*)

solid line adjoining them. In Fig. 4(b) a close-up of the two principal parametric resonances emanating from $f = 2f_1$ and $f = 2f_2$ is shown. By comparing in Fig. 5 the perturbation predictions for the transition curves with the numerical and experimental results of Fig. 4, the agreement can be considered reasonably

good given the difficulty inherent in the identification of the level of damping and the challenge associated with the experimental detection of the exact onset of the dynamic instability.

The experimentally obtained results for the parametric resonance of the in-phase mode indicate that the critical amplitude is $Y_1^c \sim 0.7$ cm at the critical frequency $f \sim 2.9$ Hz. On the other hand, for the parametric resonance of the out-of-phase mode, the critical amplitude is $Y_2^c > Y_1^c$ while the critical frequency is $f \sim 4.8$ Hz. The transition curves intersect at $Y^m \sim 1.75$ cm when $f^m \sim 3.5$ Hz. Indeed these three points in the parameter plane, (Y_1^c, f_1^c), (Y_2^c, f_2^c), (Y^m, f^m), are three characteristic points of the transition curves associated with the principal parametric resonances since they represent two local minima and a local maximum. These points can be used for the identification of damping in the pendulum. Therefore, we first determined the damping coefficients $c_1 = c_2$ that better reproduce the transition curves having first (Y_1^c, f_1^c) as reference point and, subsequently, having the value of (Y^m, f^m) as reference point.

In Fig. 4(b), the zoomed-in view in the parameter plane shows that the transition curves (dashed line), obtained with $c = c^{(3)} = 500$ g cm^2/s, reproduce well the thresholds but deviate from the rest of the experimental data. This damping coefficient corresponds to damping ratios of 2.05 % for mode 1 and 1.22 % for mode 2, respectively. These ratios can be regarded as high modal damping ratios for a pendulum problem since it is often weakly damped when the pivot is sufficiently lubricated and smooth.

With $c = c^{(2)} = 150$ g cm^2/s (damping ratios 0.62 % for mode 1 and 0.37 % for mode 2), the gray line shows a better description for most of the experimental transition curves, but not at the threshold values. This is likely due to the difficulty in capturing experimentally the threshold amplitudes with sufficient accuracy.

Since the numerical simulations with $c = c^{(3)} = 500$ g cm^2/s turn out to attenuate strongly the resonances with $m = 2$ (i.e., $\Omega \approx \omega_k$) and do not describe the experimental data adequately, apart from the threshold (Y_1^c, f_1^c) we refer to this case as the high-damping case; on the other hand, $c = c^{(2)} = 150$ g cm^2/s is referred to as the low-damping case.

The direct numerical integration for all lattice points in the parameter plane yielded also the boundaries of the regions of stabilization of the three unstable fixed points, $(0, \pi)$, $(\pi, 0)$, and (π, π). These stability regions are bounded, respectively, by the dashed lines, the dashed-dotted lines, and the dotted lines in Fig. 3(a). In the experiments, initial conditions in the neighborhoods of the unstable equilibria were given and the frequency was varied in the direction of the boundary. The experimental results are represented by the squares, circles, and stars, respectively. Most remarkably, we observe that the stability region of (π, π) is embedded in the $(\pi, 0)$-region which, in turn, is also embedded in the $(0, \pi)$-region. Above 14 Hz, there exists a small region represented by the hatching in Fig. 3(a) in which all stable regions overlap, thus all fixed points turn out to be stable. There is a large region where no overlapping of the stability regions exists; therein none of the fixed points can be rendered stable by the high-frequency excitation.

3.1 Bifurcation scenarios with high damping

The bifurcations occurring across the transition curves of the trivial state are investigated by employing a numerical continuation package [30]. The bifurcation diagrams portray variation of the amplitude of the periodic orbit—here represented by $\theta_1(t)$—with the frequency f. These bifurcation diagrams, obtained for different excitation amplitudes and $c = c^{(3)} = 500$ g cm$^2/s$, are shown in Fig. 6.

For the low amplitude, $Y = 0.97$ cm (Fig. 6(a)), by decreasing the excitation frequency, the trivial solution undergoes a supercritical pitchfork at A leading to a parametric-resonant in-phase motion which is stable up to B where a fold bifurcation is responsible for a jump to the trivial solution. By increasing the frequency, the trivial solution suffers a subcritical pitchfork bifurcation at C where a jump to the parametric-resonance solution occurs. On the other hand, the trivial solution undergoes supercritical pitchfork bifurcations into the parametric-resonance out-of-phase motion at D and E, hence no jumps are encountered by the parametric-resonance out-of-phase motions.

For a higher excitation, $Y = 1.1$ cm (Fig. 6(b)), the parametric-resonance out-of-phase motion undergoes a fold at E and a subcritical pitchfork bifurcation at F. On the other hand, in Fig. 6(b), at $Y = 1.53$ cm the branches of the in-phase and out-of-phase modes appear to be merged. To investigate the transition between the disconnected branches and their merging, a set of bifurcation diagrams is shown in Fig. 6(c) for various excitation amplitudes, $Y = (0.97, 1.1, 1.5, 1.5185, 1.53)$ cm. At some threshold

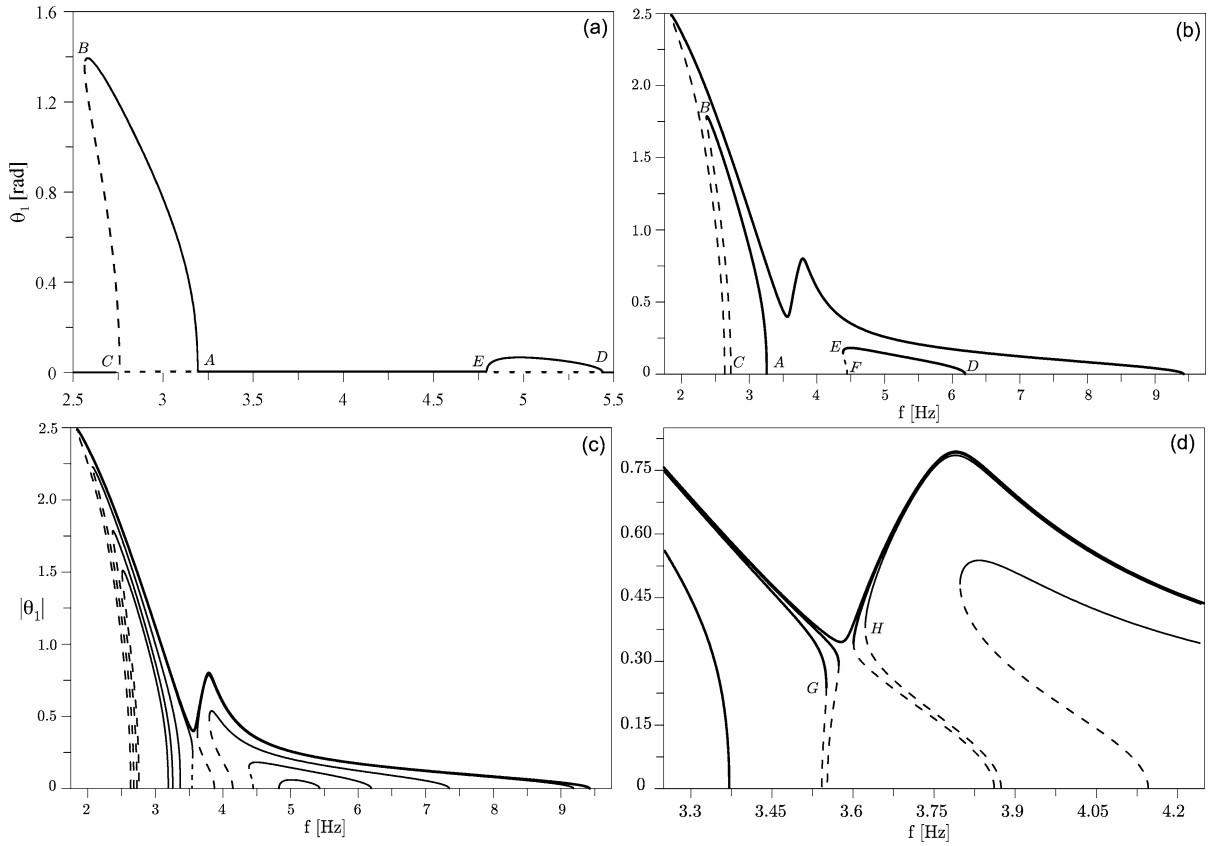

Fig. 6 Continuation-based bifurcation diagrams showing the amplitude of arm 1 vs. the excitation frequency when $Y = (0.97, 1.1, 1.5, 1.5185, 1.53)$ cm and $c = c^{(3)} = 500\ \mathrm{g\,cm^2/s}$

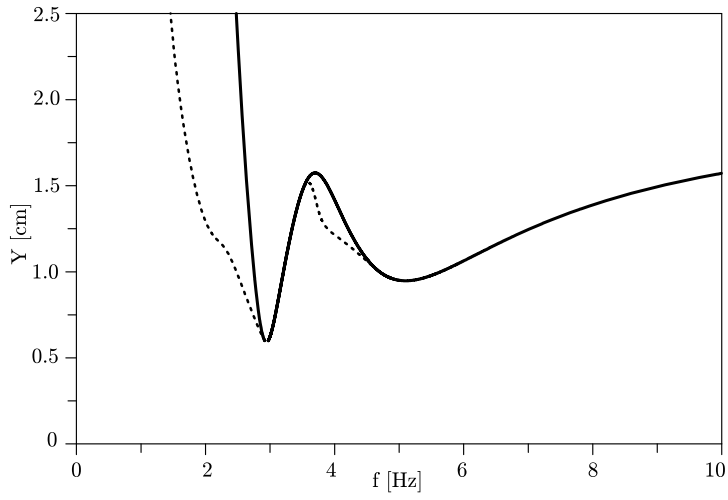

Fig. 7 Loci of the fold (*dashed lines*) and pitchfork bifurcations (*solid lines*) obtained by a continuation tool when $c = c^{(3)} = 500\ \mathrm{g\,cm^2/s}$

value, the supercritical pitchfork of the in-phase mode turns into a subcritical pitchfork with a simultaneous appearance of a fold to its right. This is better observed in Fig. 6(d). The distance between the fold of the in-phase mode (G) and that of the out-of-phase mode (H) tends to vanish at some critical amplitude at

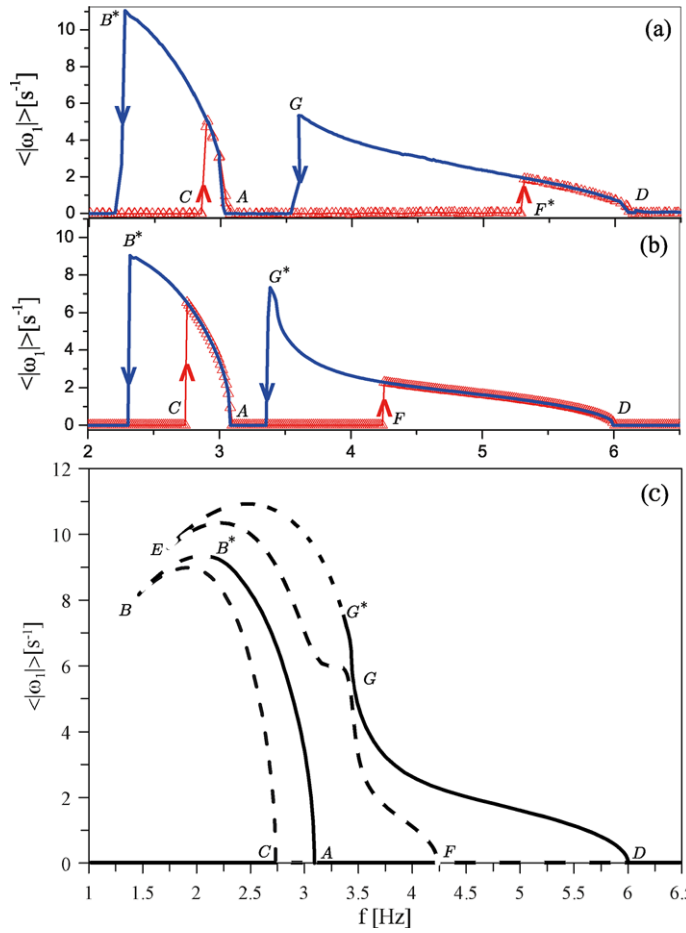

Fig. 8 (**a**) The experimentally obtained $\langle|\omega_1|\rangle$ vs. f curves for $Y = 0.75$ cm. (**b**) Numerical results and (**c**) continuation-based bifurcation diagram when $Y = 0.75$ cm and $c^{(2)} = 150\ \mathrm{g\,cm^2/s}$

which they collide and the branches become a single-connected branch. The full picture in terms of instability regions can be gained if a continuation of the pitchfork and fold bifurcations is carried out. Figure 7 shows that the nonlinearity plays a major role in determining the multi-stable region between the loci of fold bifurcations (dashed lines) and those of pitchfork bifurcations (solid lines).

3.2 Bifurcation scenarios with low damping

The parameter plane presented in Fig. 3 shows that the experimental data are better described when we consider the weaker damping value of $c^{(2)} = 150\ \mathrm{g\,cm^2/s}$ which corresponds to modal damping ratios equal to 0.62 % for mode 1 and 0.37 % for mode 2, respectively. To characterize the loss of stability of the trivial solution for some fixed values of Y, we recorded the average of the absolute value of the angular velocity ω_1 (arm 1) in forward and backward frequency sweeps. The average angular velocity $\langle|\omega_1|\rangle$ was obtained considering the last 5 % portion of the time history (with a minimum time span of 2000 s).

In Fig. 8(a) the experimentally obtained bifurcation diagrams, portraying $\langle|\omega_1|\rangle$ versus f, are shown for $Y = 0.75$ cm, slightly above the experimental threshold Y_1^c. The jumps are clearly highlighted by the arrows.

These experimental results can be well described by direct numerical integration of the equations of motion with damping coefficient $c^{(2)} = 150\ \mathrm{g\,cm^2/s}$, as shown in Fig. 8(b), where the initial conditions for each integration were taken as the end values of the state variables of the previous integration. Furthermore, the bifurcation diagrams were also obtained by continuation as shown in Fig. 8(c).

At B* and G*, the in-phase and out-of-phase modes lose their stability likely due to symmetry-breaking bifurcations.

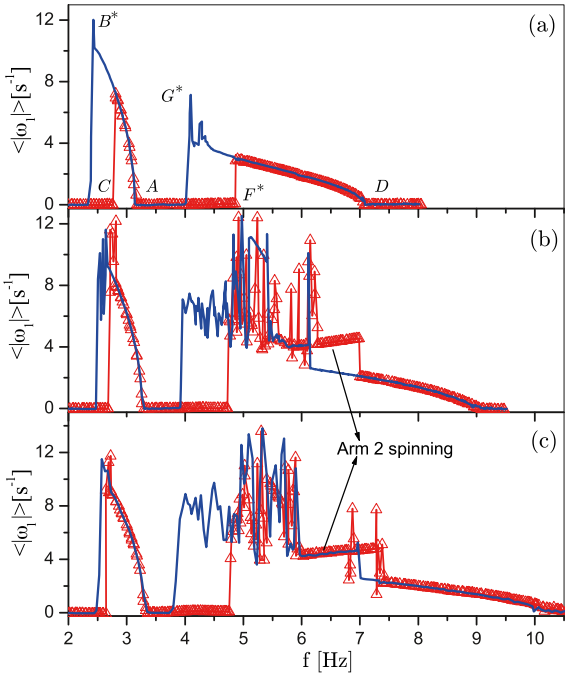

Fig. 9 Experimentally obtained bifurcation diagrams for (**a**) $Y = 1.00$ cm, (**b**) $Y = 1.35$ cm, (**c**) $Y = 1.50$ cm

For higher values of Y, the supercritical bifurcations A and D persist up to $Y^{\max} \gtrsim 1.75$ cm as shown in Figs. 9 and 10. The sudden loss of stability at the subcritical bifurcations makes the pendulum spin chaotically. As the initial conditions at the jumps happen to be the angles and angular velocities at the instant when the speed motor (i.e., excitation frequency) was varied, they are not within the basin of attraction of the limit cycles. Therefore, to avoid such sustained spinning of the pendulum, a hanging foam-type punching bag was used to reverse the rotation of arm 1 at $\theta_1 \sim \pm\pi$. The transfer of energy from the pendulum to the foam punching bag stops the spinning when the basin of attraction of the limit cycles can be achieved and the pitchfork supercritical evolution is resumed, as shown in Fig. 9(a). However, the punching bag does not act to avoid the rotation of arm 2 while arm 1 oscillates around the fixed point, as illustrated in Figs. 9(b) and 9(c). In this case, to recover the periodic solution, manual adjustments of the initial conditions were necessary.

For $Y = 1.75$ cm and with $c^{(2)} = 150$ g cm^2/s, the experimentally and numerically obtained bifurcation diagrams are shown in Fig. 10. The experimentally obtained results could be reasonably well reproduced by direct numerical integration of the equations of motion shown in Fig. 10(b), obtained by arresting the integration when the angle $|\theta_1|$ is greater than π, thus mimicking the action of the punching bag.

4 Discussion and conclusions

The phenomenon of dynamic loss of stability of the trivial downward equilibrium of a parametrically excited double pendulum (arms hanging downward in the direction of gravity) can occur through the parametric resonance of the individual modes about this trivial state or through a couple-mode parametric resonance. Thus the double pendulum, by virtue of the relatively simple mechanical context, lends itself to the study of fundamental properties inherent in the dynamic loss of stability experienced by more or less closely spaced modes of distributed-parameter systems governed by PDEs. Moreover, the double pendulum possesses three unstable equilibria when one or both arms are in the upward position. While the parametric effect of the base motion can be detrimental when causing a parametric resonance resulting into large-amplitude oscillations about the trivial state, it turns out to be beneficial when the frequency is sufficiently high since it can stabilize the unstable upright equilibrium states.

By employing theoretical and experimental approaches, it has been shown that (i) the instability regions arising from the parametric resonances can be well described by a higher-order approximation based on the method of multiple scales, (ii) the unfolding of the bifurcations via continuation and numerical simulations shows interesting scenarios. Above a certain excitation, the (right) supercritical pitchfork bifurcation of the in-phase mode becomes supercritical with a simultaneous appearance of a fold to its right. At a certain threshold excitation, this fold collides with the fold of the out-of-phase mode thus causing the two branches to coalesce into one single connected branch. The frequency band of the resonance widens abruptly spanning both modes.

The scenario becomes more complicated at lower damping values. The jumps that occur at the subcritical pitchfork bifurcations lead to chaotic solutions in which the pendulum revolves completely in two directions.

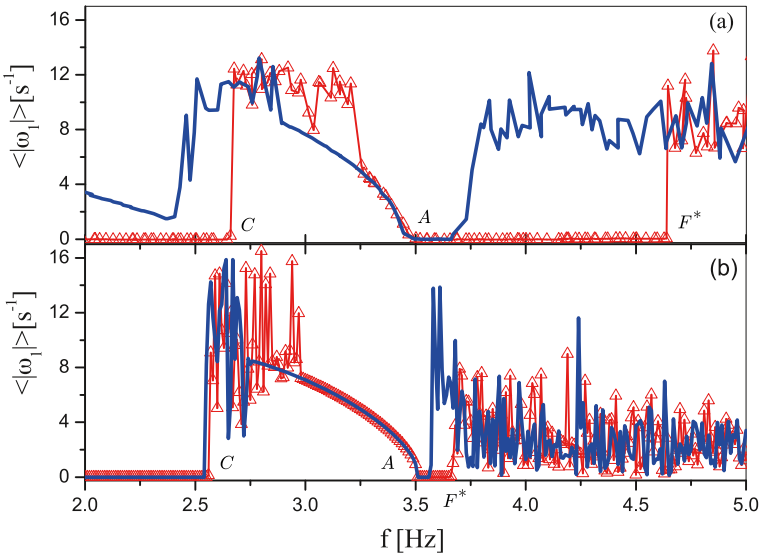

Fig. 10 (**a**) The experimentally obtained $\langle|\omega_1|\rangle$ vs. f curves for $Y = 1.75$ cm. (**b**) Numerically obtained curves with $c^{(2)} = 150\ \mathrm{g\,cm^2/s}$

Another interesting experimental finding is that there exists a region in the plane of the excitation frequency and amplitude where all three unstable equilibria can be stabilized by the parametric high-frequency excitation. In particular, by determining the boundaries of the stabilization regions of the unstable equilibrium states, we found that the stable region of the fixed point (π, π) is embedded in the $(\pi, 0)$-region which, in turn, is also embedded in the $(0, \pi)$-region, and for $f \gtrsim 14$ Hz, all of these regions overlap with the stable region of the trivial state $(0, 0)$. We also observed a large region, in which there is no overlapping, hence all fixed upright equilibrium states cannot be stabilized by parametric excitations.

Future work will address the dynamic loss of stability through parametric resonances when the two modes are auto-parametrically coupled through a two-to-one or three-to-one nonlinear transfer of energy.

Acknowledgements Financial support from the Federal Brazilian agency CNPq and from the São Paulo State Agency FAPESP. The work of Lacarbonara was partially supported by a FY 2008 AST Sapienza Grant. The precious help of Mr. Andrea Arena in generating the continuation results is gratefully acknowledged.

References

1. Faraday, M.: On a peculiar class of acoustical figures; and on certain forms assumed by a group of particles upon vibrating elastic surfaces. Philos. Trans. R. Soc. Lond. A **121**, 299–340 (1831)
2. Strutt, W.: On maintained vibrations. Philos. Mag. A **15**, 229–232 (1883)
3. TerHarr, D., Kapitza, P.L. (eds.): Collected Papers of P.L. Kapitza. Pergamon Press, New York (1965), pp. 714–726
4. Bergé, P.: Order Within Chaos. Wiley, Paris (1984)
5. Smith, H.J., Blackburn, J.A., Grønbech-Jensen, N.: Stability and Hopf bifurcations in an inverted pendulum. Am. J. Phys. **60**, 903–908 (1992)
6. Sanjuán, M.A.F.: Using nonharmonic forcing to switch the periodicity in nonlinear systems. Phys. Rev. E, Stat. Nonlinear Soft Matter Phys. **58**, 4377–4382 (1998)
7. Stachowiak, T., Okada, T.: A numerical analysis of chaos in the double pendulum. Chaos Solitons Fractals **29**, 417–422 (2006)
8. Awrejcewicz, J., Kudra, G., Lamarque, C.H.: Numerical prediction and experimental observation of triple pendulum dynamics. Int. J. Bifurc. Chaos Appl. Sci. Eng. **14**, 4191–4213 (2004)
9. Miles, J.: Parametric excitation of an internally resonant double pendulum. Z. Angew. Math. Phys. **36**, 337–345 (1985)
10. Skeldon, A.C.: Dynamics of a parametrically excited double pendulum. Physica D **75**, 541–558 (1994)
11. Agafonov, S.A., Shcheglov, G.A.: On the stabilization of a double pendulum acted upon by a follower force by means of parametric excitation. Mech. Solids **38**, 27–35 (2003)
12. El-Bassiouny, A.F.: Parametric excitation of internally resonant double pendulum. Phys. Scr. **76**, 173–186 (2007)
13. Kholostova, O.V.: On the motions of a double pendulum with vibrating suspension point. Mech. Solids **44**, 184–197 (2009)
14. Skeldon, A.C., Mullin, T.: Mode interaction in a double pendulum. Phys. Lett. A **166**, 225–229 (1992)
15. Jäckel, P., Mullin, T.: A numerical and experimental study of codimension 2 points in a parametrically excited double pendulum. Philos. Trans. R. Soc. Lond. A **454**, 3257–3274 (1998)

16. Nagamine, T., Sato, T., Koseki, Y.: Stable rotation of a parametrically excited double pendulum. J. Vib. Control **13**, 111–124 (2007)
17. Liang, Y., Feeny, B.F.: Parametric identification of a chaotic base-excited double pendulum experiment. Nonlinear Dyn. **52**, 181–197 (2008)
18. Jensen, J.S.: Non-linear dynamics of the follower-loaded double pendulum with added support-excitation. J. Sound Vib. **215**, 125–142 (1998)
19. Blekhman, I.I.: Vibrational Mechanics—Nonlinear Dynamic Effects, General Approach, Applications. World Scientific, Singapore (2000)
20. Yu, P., Bi, Q.: Analysis of non-linear dynamics and bifurcations of a double pendulum. J. Sound Vib. **217**, 691–736 (1998)
21. Kholostova, O.V.: On the motions of a double pendulum with vibrating suspension point. Mech. Solids **44**, 184–197 (2009)
22. Kholostova, O.V.: Stability of periodic motions of the pendulum with a horizontally vibrating suspension point. Mech. Solids **32**, 29–33 (1997)
23. Bardin, B.S., Markeyev, A.P.: The stability of the equilibrium of a pendulum for vertical oscillations of the point of suspension. Int. J. Appl. Math. Mech. **59**, 879–886 (1995)
24. Nayfeh A.H.: Parametric excitation of two internally resonant oscillators. J. Sound Vib. **119**, 95–109 (1987)
25. Nayfeh, A.H., Pai, F.: Non-linear non-planar parametric responses of an inextensional beam. Int. J. Non-Linear Mech. **24**, 139–158 (1989)
26. Lacarbonara, W., Antman, S.S.: Parametric instabilities of the radial motions of nonlinearly viscoelastic shells subject to pulsating pressures. Int. J. Non-Linear Mech. (2011, submitted)
27. Formalõskii, A.M.: Global stabilization of a double inverted pendulum with control at the hinge between the links. Mech. Solids **43**, 687–697 (2008)
28. Lacarbonara, W., Yabuno, H., Hayashi, K.: Nonlinear cancellation of the parametric resonance in elastic beams: Theory and experiment. Int. J. Solids Struct. **44**, 2209–2224 (2007)
29. Nayfeh, A.H., Mook, D.T.: Nonlinear Oscillations. Wiley, New York (1979)
30. Dankowicz, H., Schilder, F.: An extended continuation problem for bifurcation analysis in the presence of constraints. J. Comput. Nonlinear Dyn. **6**, 031003 (2011)
31. Nayfeh, A.H., Balachandran, B.: Applied Nonlinear Dynamics. Wiley, New York (1995)